

# New air fluorescence detectors employed in the Telescope Array experiment

H. Tokuno<sup>a,\*</sup>, Y. Tameda<sup>b</sup>, M. Takeda<sup>b</sup>, K. Kadota<sup>c</sup>, D. Ikeda<sup>b</sup>,  
M. Chikawa<sup>d</sup>, T. Fujii<sup>e</sup>, M. Fukushima<sup>b,f</sup>, K. Honda<sup>g</sup>, N. Inoue<sup>h</sup>,  
F. Kakimoto<sup>a</sup>, S. Kawana<sup>h</sup>, E. Kido<sup>b</sup>, J. N. Matthews<sup>i</sup>, T. Nonaka<sup>b</sup>,  
S. Ogio<sup>e</sup>, T. Okuda<sup>e</sup>, S. Ozawa<sup>j</sup>, H. Sagawa<sup>b</sup>, N. Sakurai<sup>e</sup>, T. Shibata<sup>b</sup>,  
A. Taketa<sup>k</sup>, S. B. Thomas<sup>i</sup>, T. Tomida<sup>g</sup>, Y. Tsunesada<sup>a</sup>, S. Udo<sup>l</sup>,  
T. Abu-zayyad<sup>i</sup>, R. Aida<sup>g</sup>, M. Allen<sup>i</sup>, R. Anderson<sup>i</sup>, R. Azuma<sup>a</sup>,  
E. Barcikowski<sup>i</sup>, J.W. Belz<sup>i</sup>, D.R. Bergman<sup>i</sup>, S.A. Blake<sup>i</sup>, R. Cady<sup>i</sup>,  
B.G. Cheon<sup>m</sup>, J. Chiba<sup>n</sup>, E.J. Cho<sup>m</sup>, W.R. Cho<sup>o</sup>, H. Fujii<sup>p</sup>, T. Fukuda<sup>a</sup>,  
D. Gorbunov<sup>q</sup>, W. Hanlon<sup>i</sup>, K. Hayashi<sup>a</sup>, Y. Hayashi<sup>e</sup>, N. Hayashida<sup>l</sup>,  
K. Hibino<sup>l</sup>, K. Hiyama<sup>b</sup>, T. Iguchi<sup>a</sup>, K. Ikuta<sup>g</sup>, T. Ishii<sup>g</sup>, R. Ishimori<sup>a</sup>,  
D. Ivanov<sup>i,r</sup>, S. Iwamoto<sup>g</sup>, C.C.H. Jui<sup>i</sup>, O. Kalashev<sup>q</sup>, T. Kanbe<sup>g</sup>,  
K. Kasahara<sup>j</sup>, H. Kawai<sup>s</sup>, S. Kawakami<sup>e</sup>, H.B. Kim<sup>m</sup>, H.K. Kim<sup>o</sup>,  
J.H. Kim<sup>m</sup>, J.H. Kim<sup>t</sup>, K. Kitamoto<sup>d</sup>, K. Kobayashi<sup>n</sup>, Y. Kobayashi<sup>a</sup>,  
Y. Kondo<sup>b</sup>, K. Kuramoto<sup>e</sup>, V. Kuzmin<sup>q</sup>, Y.J. Kwon<sup>o</sup>, S.I. Lim<sup>v</sup>,  
S. Machida<sup>a</sup>, K. Martens<sup>f</sup>, J. Martineau<sup>i</sup>, T. Matsuda<sup>p</sup>, T. Matsuura<sup>a</sup>,  
T. Matsuyama<sup>e</sup>, I. Myers<sup>i</sup>, M. Minamino<sup>e</sup>, K. Miyata<sup>n</sup>, H. Miyauchi<sup>e</sup>,  
Y. Murano<sup>a</sup>, T. Nakamura<sup>u</sup>, S.W. Nam<sup>v</sup>, M. Ohnishi<sup>b</sup>, H. Ohoka<sup>b</sup>, K. Oki<sup>b</sup>,  
D. Oku<sup>g</sup>, A. Oshima<sup>e</sup>, I.H. Park<sup>v</sup>, M.S. Pshirkov<sup>w</sup>, D. Rodriguez<sup>i</sup>,  
S.Y. Roh<sup>t</sup>, G. Rubtsov<sup>q</sup>, D. Ryu<sup>t</sup>, A.L. Sampson<sup>i</sup>, L.M. Scott<sup>r</sup>, P.D. Shah<sup>i</sup>,  
F. Shibata<sup>g</sup>, H. Shimodaira<sup>b</sup>, B.K. Shin<sup>m</sup>, J.I. Shin<sup>o</sup>, T. Shirahama<sup>h</sup>,  
J.D. Smith<sup>i</sup>, P. Sokolsky<sup>i</sup>, T.J. Sonley<sup>i</sup>, R.W. Springer<sup>i</sup>, B.T. Stokes<sup>i</sup>,  
S.R. Stratton<sup>i,r</sup>, T. Stroman<sup>i</sup>, S. Suzuki<sup>p</sup>, Y. Takahashi<sup>b</sup>, M. Takita<sup>b</sup>,  
H. Tanaka<sup>e</sup>, K. Tanaka<sup>x</sup>, M. Tanaka<sup>p</sup>, G.B. Thomson<sup>i</sup>, P. Tinyakov<sup>q,w</sup>,  
I. Tkachev<sup>q</sup>, S. Troitsky<sup>q</sup>, K. Tsutsumi<sup>a</sup>, Y. Tsuyuguchi<sup>g</sup>, Y. Uchihori<sup>y</sup>,  
H. Ukai<sup>g</sup>, G. Vasiloff<sup>i</sup>, Y. Wada<sup>h</sup>, T. Wong<sup>i</sup>, M. Wood<sup>i</sup>, Y. Yamakawa<sup>b</sup>,  
H. Yamaoka<sup>p</sup>, K. Yamazaki<sup>e</sup>, J. Yang<sup>v</sup>, S. Yoshida<sup>s</sup>, H. Yoshii<sup>z</sup>,  
R. Zollinger<sup>i</sup>, Z. Zundel<sup>i</sup>

<sup>a</sup>*Tokyo Institute of Technology, Meguro, Tokyo, Japan*

<sup>b</sup>*Institute for Cosmic Ray Research, University of Tokyo, Kashiwa, Chiba, Japan*

<sup>c</sup>*Tokyo City University, Setagaya-ku, Tokyo, Japan*

---

\*Corresponding author. Tel.: +81-357342462, Fax: +81-357342756. E-mail address: htokuno@cr.phys.titech.ac.jp (H. Tokuno).

- <sup>d</sup>*Kinki University, Higashi Osaka, Osaka, Japan*  
<sup>e</sup>*Osaka City University, Osaka, Osaka, Japan*  
<sup>f</sup>*University of Tokyo, Institute for the Physics and Mathematics of the Universe,  
Kashiwa, Chiba, Japan*  
<sup>g</sup>*University of Yamanashi, Interdisciplinary Graduate School of Medicine and  
Engineering, Kofu, Yamanashi, Japan*  
<sup>h</sup>*Saitama University, Saitama, Saitama, Japan*  
<sup>i</sup>*University of Utah, High Energy Astrophysics Institute, Salt Lake City, Utah, USA*  
<sup>j</sup>*Waseda University, Advanced Research Institute for Science and Engineering,  
Shinjuku-ku, Tokyo, Japan*  
<sup>k</sup>*Earthquake Research Institute, University of Tokyo, Bunkyo-ku, Tokyo, Japan*  
<sup>l</sup>*Kanagawa University, Yokohama, Kanagawa, Japan*  
<sup>m</sup>*Hanyang University, Seongdong-gu, Seoul, Korea*  
<sup>n</sup>*Tokyo University of Science, Noda, Chiba, Japan*  
<sup>o</sup>*Yonsei University, Seodaemun-gu, Seoul, Korea*  
<sup>p</sup>*Institute of Particle and Nuclear Studies, KEK, Tsukuba, Ibaraki, Japan*  
<sup>q</sup>*Institute for Nuclear Research of the Russian Academy of Sciences, Moscow, Russia*  
<sup>r</sup>*Rutgers University, Piscataway, USA*  
<sup>s</sup>*Chiba University, Chiba, Chiba, Japan*  
<sup>t</sup>*Chungnam National University, Yuseong-gu, Daejeon, Korea*  
<sup>u</sup>*Kochi University, Kochi, Kochi, Japan*  
<sup>v</sup>*Ewha Womans University, Seodaaemun-gu, Seoul, Korea*  
<sup>w</sup>*University Libre de Bruxelles, Brussels, Belgium*  
<sup>x</sup>*Hiroshima City University, Hiroshima, Hiroshima, Japan*  
<sup>y</sup>*National Institute of Radiological Science, Chiba, Chiba, Japan*  
<sup>z</sup>*Ehime University, Matsuyama, Ehime, Japan*

---

## Abstract

Since 2007, the Telescope Array (TA) experiment, based in Utah, USA, has been observing ultra high energy cosmic rays to understand their origins. The experiment involves a surface detector (SD) array and three fluorescence detector (FD) stations. FD stations, installed surrounding the SD array, measure the air fluorescence light emitted from extensive air showers (EASs) for precise determination of their energies and species. The detectors employed at one of the three FD stations were relocated from the High

Resolution Fly’s Eye experiment. At the other two stations, newly designed detectors were constructed for the TA experiment. An FD consists of a primary mirror and a camera equipped with photomultiplier tubes. To obtain the EAS parameters with high accuracies, understanding the FD optical characteristics is important. In this paper, we report the characteristics and installation of new FDs and the performances of the FD components. The results of the monitored mirror reflectance during the observation time are also described in this report.

*Keywords:* Ultra high energy cosmic rays, Extensive air showers, Air fluorescence light detectors

---

## 1. Introduction

The Telescope Array project is a collaboration with 120 scientists from four nations (Japan, USA, Korea, and Russia), with the observatory located in Utah, USA [1, 2]. The detectors involved in the Telescope Array experiment consist of surface detectors (SDs) arranged in an array and fluorescence detector (FD) telescopes. Fig. 1 shows the detector map (squares: SD positions, triangles: FD station positions). The SD array consists of 507 SDs, arranged over an area of approximately 700 km<sup>2</sup> with 1.2 km spacing between the SDs [4]. The SDs measure the arrival timing and particle densities of extensive air showers (EASs) using two-layered plastic scintillators of 3 m<sup>2</sup>. Three FD stations are placed around the SD array. The FDs measure the air fluorescence light emitted from EASs; the FD data are analyzed and the longitudinal development of EASs is reconstructed to estimate primary energies, arrival directions, and particle species with the aim of studying the

15 nature of ultra high energy cosmic rays.

16 The FD station near the northwest corner of the SD array houses fourteen  
17 FDs that were relocated from the High Resolution Fly’s Eye (HiRes) experi-  
18 ment (e.g. [3]). For these FDs and for the data obtained using these FDs, we  
19 can use the same calibration and analysis methods used in the HiRes experi-  
20 ment [5]. The specifications, configurations, and calibrations of the relocated  
21 FDs can be obtained from previous reports on HiRes (e.g. [3]). On the other  
22 hand, the southeast (BRM) and southwest (LR) FD sites have twelve FDs  
23 each; these FDs were newly designed for the TA experiment. A picture of  
24 the FD station is shown in Fig. 2.

25 An FD consists of a primary mirror and a photomultiplier tube (PMT)  
26 camera. We employed a spherical mirror to obtain a wide field of view (FOV)  
27 with a sufficient focusing power. In addition, the size of the collecting area  
28 of the mirror was determined from the maximum distance for detectable  
29 EASs at the highest energies. The mirror aperture and curvature radius  
30 were determined to be 3300 mm (area of 6.8 m<sup>2</sup>) and 6067 mm, respectively.  
31 This setting realizes the detection of EASs with a sufficiently high accuracy  
32 from a distance of 30 km and with the primary energy of 10<sup>20</sup> eV.

33 A primary mirror is segmented into eighteen small hexagonal mirrors;  
34 the distance between the parallel sides of the hexagonal mirror was 660 mm.  
35 A PMT camera consisting of 16×16 PMTs and having an effective area of  
36 860 mm × 992 mm is set at a distance of 3000 mm from the mirror. The FOV  
37 of each PMT is approximately 1°, and that of the camera is 15° in elevation  
38 and 18° in azimuth. Fig. 3 shows a schematic view of the FD telescope  
39 frame equipped with a pair of telescopes, one each in the upper and lower

40 parts of the frame. The heights of the upper and lower mirror centers and  
41 the upper and lower camera centers from the floor are 5.5, 1.5, 6.0, and  
42 2.8 m, respectively. The FOV centers of the upper and lower telescopes are  
43 at elevations of  $10.5^\circ$ , and  $25.5^\circ$ , respectively. As shown in Fig. 3, no segment  
44 mirror is installed at the center of the primary mirror. At this position, a  
45 jig was mounted for alignment of the optical system of the telescope when it  
46 was constructed. Similarly, during normal operations, a UV light flasher is  
47 mounted here as a standard light source for the calibrations and adjustments  
48 of PMT gains [6]. The projected view of the FD station onto the station  
49 floor is shown in Fig. 4. The station has six telescope frames; accordingly,  
50 the FOV of a station is from  $3^\circ$  to  $33^\circ$  in elevation and  $108^\circ$  in azimuth.

51 To evaluate the accuracies of the measured shower parameters such as  
52 arrival direction, primary energy, and longitudinal development, studies of  
53 resolutions and systematic uncertainties of FD telescope optics are impor-  
54 tant. Thus, we ensured that we accurately manufactured, constructed, and  
55 installed the FD telescopes with utmost care and after confirmation of their  
56 optical characteristics.

57 In this paper, we describe the elements that constitute an FD telescope  
58 and the installation process of the telescopes. Moreover, the reflectance of  
59 segment mirrors, which are continuously monitored after the installations,  
60 is also presented. The contents of this paper are as follows. In Sec. 2 and  
61 Sec. 3, we report the designs and productions of the PMT cameras and those  
62 of the segment mirrors, respectively. Sec. 4 explains the installation of the  
63 cameras and mirrors. Mirror reflectance and its variations are described in  
64 Sec. 5.

## 65 **2. Camera production**

66 In this section, we describe the configuration of the newly designed PMT  
67 cameras and the results of user acceptance tests.

### 68 *2.1. Photomultiplier tube*

69 Each camera has 256 PMTs. 7000 PMTs including spares have been  
70 produced. The PMT used in the TA experiment, Hamamatsu R9508 based  
71 on R6234-01, is specially manufactured for the experiment. The photoelectric  
72 surface on the top of a tube is hexagonal in shape with a distance of 60 mm  
73 between the parallel side; its effective area is equivalent to that of circle of  
74 57 mm diameter [6]. On the bottom of the tube, a printed circuit board of a  
75 bleeder and a preamplifier is installed. In order to reduce the contamination  
76 of the night sky background photons into fluorescence signals, we use a 4 mm  
77 thick optical filter (SCHOTT AG, BG3). The filter is mounted on the surface  
78 of each PMT using a self-fusing tape (Hitachi Chemical Co., Ltd., HIGHBON  
79 TAPE No.2) and a polyimide film tape (3M, 5434). The transmittance of  
80 BG3 is higher than 80% in the wavelength range of 305–395 nm, which is  
81 within the range of all the major air fluorescence lines [6].

82 The PMTs were inspected by the supplier before shipping and were se-  
83 lected based on their cathode and anode sensitivities, dark current, and other  
84 basic parameters. In addition, the quantum efficiency (including collection  
85 efficiency), and cathode uniformity were measured for sampled PMTs, once  
86 for 1000 PMTs. We also imposed sufficiently high gains and low noise levels  
87 on PMTs at the experimental sites. The minimum required gain was  $6 \times 10^4$   
88 with the maximum applied high voltage of  $-1200$  V.

89 After installation of camera, we adjusted PMT gains to absolutely cali-  
90 brated PMTs [7] and measured the uniformity of the PMT response at its  
91 photoelectric surface on the sites [6]. During FD observations, each PMT  
92 gain was monitored every one hour using UV flashers. We exchanged two of  
93 the 6144 PMTs because the gains of these two PMTs had decreased in the  
94 first half year. Since then, no PMT has been exchanged.

## 95 *2.2. Camera*

96 A PMT camera has been placed at the primary focus of each FD telescope.  
97 Fig. 5 shows the schematic view of the PMT camera. The camera has a UV  
98 transparent acrylic window (KURARAY, PARAGLAS-UV00) attached in  
99 front of PMTs for protection from dust. The transmittance of the window  
100 is more than 90% in the wavelength range of 300–400 nm [6]. PMTs were  
101 fixed on a 16 mm thick plate of extra super duralumin and were arranged on  
102 a triangular grid with a clearance gap of approximately 1 mm among them.  
103 The gap geometries were measured based on the uniformity of the camera  
104 surface response [6].

105 Signals from the PMTs and the DC power to the PMTs are transferred  
106 through shielded LAN cables of category 5 (length: 50–100 cm) between the  
107 PMTs and the patch panels inside a camera. The patch panels connected  
108 to the LAN cables are shown in Fig. 6. We use a shielded 40 core twisted  
109 pair cable (Bando Densen Co., Ltd., BIOS-A-2820P) each for sixteen PMTs  
110 to transfer the PMT signals from the patch panels in a camera to a data  
111 acquisition (DAQ) system in the electronics room with temperature control,  
112 situated 20 m from the camera location. The cable length for the upper and  
113 lower cameras is 25.5 m and 22.3 m, respectively. Detailed descriptions of

114 the electronics and DAQ system are presented elsewhere [8, 9].

115 High voltages (HVs) are applied to PMTs via coaxial cables (Bando  
116 Densen Co., Ltd., 1.5D-2V) using an order-made power supply (Takasago  
117 Co., Ltd.). The power supply has 256 outputs, and HV value on each out-  
118 put can be controlled and monitored separately through Ethernet, with the  
119 accuracy of  $\pm 0.2\%$ . This uncertainty corresponds to approximately  $\pm 2\%$   
120 of the PMT gains under our setting. The typical applied HV to PMTs is  
121  $-880$  V, and the rated maximum voltage is  $-1200$  V. As a safety measure  
122 to protect human beings, PMTs, and the power supply, the power supply is  
123 automatically shut down when unusually high values are detected.

124 A DC power supply (KENWOOD, PW18-3AD) is connected to two patch  
125 panels to distribute DC voltage of  $\pm 5$  V to the 256 preamplifiers, each con-  
126 nected to one PMT. In this manner, we prepared one DC power supply for  
127 each camera.

### 128 **3. Segment mirrors and their production**

129 In this section, we describe the specifications of the segment mirrors em-  
130 ployed in the new FD telescopes of the TA experiment, their pre-shipment  
131 and acceptance inspections, and the inspection results.

#### 132 *3.1. Segment mirrors*

133 The 3.3 m aperture spherical mirror of the FD telescope is segmented into  
134 eighteen small mirrors, as shown in Fig. 3. The mirror is made of borosilicate  
135 glass (SCHOTT AG, TEMPAX), and each segment is hexagonal in shape  
136 with a thickness of 10.5 mm and a distance of 660 mm between the parallel  
137 sides. On the surface of the mirror was deposited a 200 nm thick reflection



138 coating of aluminum through vacuum deposition, and on this coating was  
139 deposited a 50 nm thick protective coating of  $\text{Al}_2\text{O}_3$  through anodization  
140 process. The wavelength that induces maximum reflectance depends on the  
141 thickness of the anodized coating. This thickness was optimized to obtain  
142 the maximum reflectance at wavelength of 350 nm.

143 The optical parameters and fabrication accuracies of segment mirrors de-  
144 pend on the experimental requirement. In order to optimize the optical  
145 parameters, we studied the reconstruction accuracies of EASs using ray-  
146 tracing, EAS simulation, and reconstruction programs. From our studies,  
147 we determined the specifications of the optical parameters and the fabrica-  
148 tion accuracies; the curvature radius of the segment mirror was 6067 mm  
149  $\pm 100$  mm, the spot size at the focal point was smaller than 40 mm (it is  
150 comparable size of the PMT surface), and the reflectance in the wavelength  
151 range of 300 nm–400 nm was more than 85%.

### 152 *3.2. Segment mirror production*

153 Segment mirrors were manufactured (Sanko Seikohjyo Co., Ltd.) from  
154 January to November, 2004, for the BRM station and from March to De-  
155 cember, 2006, for the LR station. In all, 500 segment mirrors, including  
156 spares, were produced. The procedure for mirror production is as follows.  
157 First, the segment mirror was shaped by heating a planar glass on a ceramic  
158 model plate in a temperature-controlled electric oven. After this spherical  
159 mirror fabrication, the mirrors were selected through curvature radius mea-  
160 surement. Next, the mirror surface was coated with 200 nm thick aluminum  
161 through the vacuum deposition. To protect the surface, 50 nm thick  $\text{Al}_2\text{O}_3$   
162 crystal layer was coated on it; these  $\text{Al}_2\text{O}_3$  crystals were produced from a

163 solution containing ammonium hydroxide, tartaric acid, and ethylene glycol.  
164 After the surface fabrication, the mirrors were selected based on reflectance  
165 measurement. Finally, a 150 mm diameter support disk made of the same  
166 material as the mirror and a stainless steel flange were bonded to the back  
167 of the mirror using glue (3M, Dymax 840). The flange was used to support  
168 the segment mirror from the telescope frame.

### 169 *3.3. Acceptance test for curvature radius and spot size*

170 For the acceptance inspections, we measured the curvature radius and  
171 spot size at the curvature center. From our ray-tracing studies, we estimated  
172 an acceptable spot diameter of 20 mm, in which 90% of the reflected photons  
173 fall, at the center of the curvature. Because of this phenomenon, parallel  
174 incident light makes a spot of 40 mm diameter on the camera, in which 68% of  
175 reflected photons fall, in the case of a normal FD observation. We developed  
176 a test system to measure the curvature radius of mirrors as the distance  
177 corresponding to the minimum spot size. Fig. 7 shows the schematic view  
178 of the system, and Fig. 8 shows the photograph of the same. This system  
179 consisted of a linear precision motion stage (range:  $\pm 250$  mm, accuracy:  
180 0.04 mm, Chuo Precision Industrial Co.,Ltd., MM STAGE ALS-250-C2P  
181 with controller QT-CD1); a diffused light source, i.e., a green laser (Kochi  
182 Toyonaka Giken Co.,Ltd., GLM-D2) with a diffuser plate; an image scanner  
183 (range: 16 bit, resolution: 2400–4800 dpi, Canon, CanoScan LiDE80); and a  
184 laser distance meter (accuracy:  $\pm 1$  mm, Murakami Giken, DIST pro<sup>4</sup>a). The  
185 diffused light source was set 100 mm away from the optical axis of the mirror,  
186 and the center of the scanner’s sensitive area was fixed at the axisymmetrical  
187 point to the optical axis. Both the light source and the scanner were mounted

188 on the motion stage and were collectively moved between  $6067 \pm 100$  mm from  
189 the center of the mirror in 5 mm steps. Next, we determined the curvature  
190 radius by searching for the point where the spot size was minimized. From our  
191 ray-tracing calculations, we confirmed that the spot size of the light reflected  
192 on the scanner was minimized at the same distance as the curvature radius  
193 in spite of the off-axis alignments of the light source and the scanner.

194 A typical observed spot image is shown in Fig. 9. In this analysis, the  
195 image size was defined as the diameter of the circle in which 90% of the  
196 detected photons fall; this circle was centered at the weighted center of the  
197 image. Circles in Fig. 10 show an example relation between the spot size  
198 and the distance from a mirror. From the data points (circles) in Fig. 10, we  
199 obtain the curvature radius to be 6082 mm. Typically, as shown in Fig. 9,  
200 the image shape was non ideal circle, because the surface of the mirrors  
201 was slightly elliptical. Accordingly, we required an additional criterion for  
202 elliptical mirrors. We also measured spot sizes of elliptical mirrors as follows.  
203 First, we fitted a shot image at the beginning of a distance of 5967 mm  
204 with a line (called X axis), and another line (called Y axis) was obtained  
205 perpendicular to the X axis. These axes were fixed during the subsequent  
206 calculations. The shot image was projected on these axes, and the projected  
207 spot sizes on these axes were calculated at each distance step that the stage  
208 away from the mirror. Finally, we obtained the curvature radii on these axes  
209 from the minimum of these plots. We also required the curvature radii on  
210 the two axes to be within  $6067 \pm 100$  mm. The projected spot sizes on the X  
211 and Y axes for the sampled mirror are shown as square and triangle points,  
212 respectively, in Fig. 10. From this figure, the curvature radii on the X and Y

213 axes are 6072 mm and 6087 mm, respectively, and these radii also satisfy the  
214 above requirement. Fig. 11 shows the distribution of the curvature radius of  
215 the accepted mirrors, and Fig. 12 shows the distribution of the normal spot  
216 size in diameter at the curvature radius. The curvature radius of the accepted  
217 mirrors is 6057 mm ( $1\sigma$ :  $-20/+30$  mm), and their spot size is 12 mm ( $1\sigma$ :  
218  $-2/+3$  mm) in diameter. Henceforth,  $1\sigma$  indicates 68% confidence level.

219 From the acceptance test, we found that 5% mirrors were unacceptable.  
220 To complement the required number of mirrors, other acceptable mirrors  
221 were produced additionally.

#### 222 *3.4. Acceptance test for reflectance*

223 We employed two different acceptance tests for the segment mirror re-  
224 flectance. One is an accurate measurement in the laboratory for a wide  
225 wavelength range for sampled mirrors, which was performed by the manufac-  
226 turer. The other is a simple measurement with a portable spectrophotometer  
227 for a narrow wavelength range for all the segment mirrors.

228 As it is difficult to measure the reflectance of the curved and large segment  
229 mirrors accurately, the manufacturer produced small flat pieces of mirrors  
230 simultaneously with sampled segment mirrors and precisely measured the  
231 reflectance of the flat pieces as part of the delivery inspection process. The  
232 reflectance of the small flat mirrors was measured using a spectrometer (Jasco  
233 Inc., Ubest V-550), whose range, resolution, and accuracy are 190–900 nm,  
234 2 nm, and 1%, respectively. Fig. 13 shows the typical reflectance of sampled  
235 small flat mirrors. This reflectance is more than 90% in the wavelength range  
236 of 300–400 nm, containing all the major air fluorescence lines.

237 We use a portable spectrophotometer (Konica Minolta, Inc., CM-2500d)

238 for acceptance inspections of all the manufactured segment mirrors and for  
239 routine monitoring of reflectance. The range and its resolution are 360–740 nm  
240 and 10 nm, respectively. The nominal uncertainties of measurement are less  
241 than 1%. To confirm the accuracy and stability of the spectrophotometer,  
242 we measured the reflectance of a reference mirror eighteen times in the pe-  
243 riod from June 2008 to November 2010. The reference mirror (Ocean Optics  
244 Inc., STAN-SSH-NIST) is quartz-coated; its reflectance was measured by the  
245 National Institute of Standards and Technology (NIST), USA. Fig. 14 shows  
246 a comparison between our measurements and those done by NIST. From  
247 this figure, the systematic differences are within  $\pm 1\%$  and the deviations are  
248 within  $\pm 1\%$  in the concerned wavelength range. Fig. 15 shows the varia-  
249 tion in the reflectance of the reference mirror at the wavelength of 360 nm,  
250 measured using a portable spectrophotometer. The stability was 0.6% ( $1\sigma$ )  
251 during the period from June 2008 to November 2010.

252 The typical reflectance of a primary mirror composed of eighteen segments  
253 is shown in Fig. 16. This figure shows that the reflectance in the wavelength  
254 range of 360–400 nm is higher than 90%. The distribution of the reflectance  
255 at 360 nm for all the segment mirrors is shown in Fig. 17. This distribution  
256 shows that the differences in the reflectance depend on 108 sampling points  
257 of each primary mirror and that the variance is less than 1%, which is within  
258 measurement accuracies. Fig. 18 shows the reflectance of the primary mirrors  
259 in BRM and LR stations, which is the average of eighteen segment mirrors,  
260 with  $1\sigma$  error bars. All the telescopes fulfilled the requirement that the  
261 averaged reflectance was greater than 90% in the wavelength range of 360 nm.

## 262 4. Telescope installation

263 Mirrors and cameras were shipped from Japan to our observatory in Utah,  
264 USA, and these items were installed at BRM from February 2005 to July 2006  
265 and at LR in March 2007. In this section, we describe the installations of  
266 the FD telescopes and their alignment.

### 267 4.1. Installation of telescope frame

268 As shown in Fig. 4, six telescope frames were installed in each station  
269 (BRM and LR) with each frame having two telescopes. Hence, in all, twelve  
270 telescopes were installed in each station.

271 A station building has three rolling doors to protect the telescopes from  
272 sunlight, rain, wind, and other natural conditions. The telescopes are directly  
273 exposed to air during FD observation, because no other protection windows  
274 were installed.

275 When the wind speed was higher than 15 m/s, doors were closed to pre-  
276 vent themselves from being stuck. We required less than  $0.1^\circ$  FOV deflections  
277 of the telescope with wind speeds lower than 15 m/s. Wind-induced deflec-  
278 tions of the telescopes were studied by the manufacturer (Mitsui Engineering  
279 & Shipbuilding Co., Ltd.) using simulation programs and by applying wind-  
280 tunnel tests on a structure model of a station including telescopes. From  
281 their studies, winds from the side of the telescope building induce the max-  
282 imum deflections in the telescope frame. Because winds pass through the  
283 building from one door to another, their effective speed is not reduced by  
284 the building. However, the current design of the frame fulfills our require-  
285 ment with regard to frame deflections, even in the worst condition. Based

286 on the studies of the manufactures, the design of telescope frame structure  
287 was fixed.

288 To install the telescope frames precisely, we conducted a survey and drew  
289 datum lines and points for telescope geometry. Using a gyro-compass, the  
290 absolute azimuthal direction was measured with reference to a mountain's  
291 peak. Uncertainties of the gyro-compass measurement was  $1'$ , which was  
292 confirmed from the star observation using the gyro-compass. Three datum  
293 lines, shown as solid lines in Fig. 4, were drawn on the floor with relative  
294 accuracies of  $1'$  between these lines. Azimuthal lines of each telescope frame,  
295 shown as dashed lines in Fig. 4, were drawn from the datum lines with  
296 accuracies of  $0.1^\circ$  using a measuring tape. From the azimuthal lines, reference  
297 points for the telescope frames were marked with accuracies of 1 mm.

298 We installed the telescope frames, which can be separated into frames for  
299 cameras and mirrors, as shown in Fig. 3, in accordance with the following  
300 procedures. The telescope frames were placed and fixed on the reference  
301 points, and before installing real cameras, a prototype standard camera was  
302 attached to the camera frames. This prototype standard camera had the  
303 same weight and size of a real camera and was equipped with reference lines  
304 on the surface for adjusting positions. A steel cylinder with a diameter of  
305 500 mm is mounted at the center of each primary mirror, as shown in Fig. 3.  
306 The central cylinder was used to adjust the alignment of segment mirrors  
307 and the camera of the telescope.

308 Telescope directions were adjusted by the following procedures. First, we  
309 installed a laser range meter on the central cylinder. Next, we adjusted the  
310 elevation angle to the specified value, monitored using a digital tilt meter,

311 (Digital Protractor, Pro 360), with an accuracy of  $\pm 0.2^\circ$ . We adjusted the  
312 azimuthal angle of the cylinder for the central axis laser to point the string of  
313 a plumb 3000 mm away from the cylinder set exactly above the reference line  
314 on the floor. Then, the position of the camera frame was precisely adjusted  
315 with reference to the central axis laser. The upper limit for the installed error  
316 on the distance between the camera and the cylinder is  $\pm 30$  mm. However,  
317 this misalignment was resolved when we installed mounts of segment mirrors  
318 whose heights were adjusted to remove the distance error. On the other  
319 hand, to reduce the construction cost, we required relatively low accuracies  
320 of the direction of the camera, which are within  $1^\circ$ . This affects the negligible  
321 uncertainties of the effective area of the camera, the order of which is  $\cos(1^\circ)$ .  
322 After the adjustment of the camera position, the prototype standard camera  
323 was unmounted from the camera frame.

324 Finally, the positions of the segment mirror mount were adjusted. Fig. 19  
325 shows the schematic view of a jig called “BANANA1” for adjusting the posi-  
326 tions of the segment mirror mount. BANANA1 was mounted on the central  
327 cylinder of mirrors and can be rotated around the central axis of the cylin-  
328 der. The equipment had two arms, one of which had three protruding legs  
329 of different lengths; the other arm had a counter weight. By rotating BA-  
330 NANA1, we adjusted the length of every segment mirror mount for one of  
331 the three legs on BANANA1 to be aligned with the reference point on the  
332 mount surface. At the same time, the direction of each segment mirror was  
333 roughly adjusted using BANANA1.



334 *4.2. Installation of cameras and mirrors*

335 The cameras and mirrors were set on the telescope frame by the follow-  
336 ing procedures. We set the segment mirrors on their mounts and precisely  
337 aligned each direction by screwing in and out two adjusting bolts on a mount.  
338 To adjust the direction of segment mirrors, we use an equipment called “BA-  
339 NANA3”, shown in Fig. 20. The equipment was mounted on the camera  
340 frame, and a white board was perpendicularly set on the optical axis of the  
341 primary mirror. The distance between segment mirrors and the board was  
342 6067 mm, which is the same distance as the curvature radius of the mirrors.  
343 Green LEDs were connected to the white board, 5, 10, and 15 cm away from  
344 the center of curvature, as shown in Fig. 21. When the direction of the seg-  
345 ment mirror was adjusted, the LED lights were reflected to the symmetrical  
346 point about the center of curvature. The direction was adjusted with an  
347 accuracy of less than  $0.1^\circ$ , which was estimated from the accuracy of cen-  
348 ter position determination of reflected light of 5 mm (1/4 diameter of the  
349 reflected lights) and from the distance between mirror and the white board,  
350 6067 mm. For parallel lights, this setting accuracy provided us the spots  
351 of 40 mm diameter, in which 68% of reflected photons fall, at the camera  
352 surface. After these adjustments, the segment mirror mounts were locked  
353 up.

354 PMT cameras were mounted on the camera frames with an accuracy of  
355 10 mm on the camera plane. This accuracy corresponds to  $\sim 0.2^\circ$  uncer-  
356 tainty of the telescope’s pointing direction. PMT cameras were connected  
357 by signal, HV, and DC cables. Finally, the wiring was confirmed through  
358 test operations.

359 In all, the directions of the telescope are adjusted with a few  $0.1^\circ$  accura-  
360 cies. These directions were confirmed with a star light analysis, which uses a  
361 similar method as in reference [10]. Our FDs record air fluorescence signals  
362 with background photons (BGPs), as we employ a DC coupling for the PMT  
363 signal readout. Thus, we obtain the variations in BGP with a normal trigger  
364 rate of 2–3 Hz. When a star traverses the FOV of a PMT, the number of  
365 BGPs increases and decreases in a few minutes. The time variations of BGPs  
366 are simulated from star positions and telescope directions. Using these esti-  
367 mated time variations of BGPs, we studied the telescope directions and spot  
368 sizes of the primary mirror. The correction values of the FOV direction of  
369 FD obtained from this study are used in our simulation and the EAS recon-  
370 struction programs. Our results of the star light analysis will be reported in  
371 a future paper.

## 372 5. Mirror reflectance monitoring

373 The reflectance of the segment mirrors is monitored every months. Mir-  
374 ror reflectance decreases with time, because our FDs are exposed to the air  
375 directly and because dust is attached to the mirrors during observations. In  
376 addition, the reflectance of lower mirrors decreases more rapidly than that of  
377 upper mirrors. Fig. 22 shows the time variations of the averaged mirror re-  
378 flectance at 360 nm of a typical lower telescope LR04. The largest decrement  
379 of 4 % occurred between June 2007 and March 2008. When we analyze the  
380 FD data from that period, we take this 4 % as the systematic uncertainty of  
381 the mirror reflectance.

382 Every summer, the mirrors are washed using purified water and deter-

383 gent for sensitive equipments (Alconox, Inc., LIQUI-NOX). Purified water  
384 is obtained from tap water filtered through charcoal and deionization filters.  
385 After washing, the mirrors are rinsed using purified water and dried naturally.  
386 Fig. 22 shows that the reflectance of the mirror after washing is recovered  
387 to the same level as in the first installation. Fig. 23 shows the differences  
388 in mirror reflectance before and after washing at each wavelength; these dif-  
389 ferences have no clear wavelength dependencies. Based on this result, we  
390 mainly monitor the reflectance at 360 nm.

## 391 **6. Summary**

392 In Japan, we have produced PMT cameras and mirrors for use in the air  
393 fluorescence detector of the Telescope Array experiment. The cameras and  
394 mirrors that passed our acceptance inspections were shipped to our experi-  
395 mental site in Utah, USA. The telescope frames, mirrors, and cameras were  
396 installed at the FD stations. The directions of the telescope are adjusted  
397 with an accuracy of a few  $0.1^\circ$ , and the directions are confirmed with a star  
398 light analysis. These parameters are used in our detector simulation and  
399 the EAS reconstruction programs. Monitoring of the performances of the  
400 cameras and mirrors begin according to the following schedules: the gains of  
401 PMT camera, hour by hour during FD operation; mirror reflectance, every  
402 few months. Our mirrors are washed every summer, and their reflectance  
403 after washing is recovered to the same level as in the first installation.

404 **Acknowledgments**

405 The Telescope Array experiment is supported by the Japan Society for  
406 the Promotion of Science through Grants-in-Aid for Scientific Research on  
407 Specially Promoted Research (21000002) “Extreme Phenomena in the Uni-  
408 verse Explored by Highest Energy Cosmic Rays”, and the Inter-University  
409 Research Program of the Institute for Cosmic Ray Research; by the U.S.  
410 National Science Foundation awards PHY-0307098, PHY-0601915, PHY-  
411 0703893, PHY-0758342, and PHY-0848320 (Utah) and PHY-0649681 (Rut-  
412 gers); by the National Research Foundation of Korea (2006-0050031, 2007-  
413 0056005, 2007-0093860, 2010-0011378, 2010-0028071, R32-10130); by the  
414 Russian Academy of Sciences, RFBR grants 10-02-01406a and 11-02-01528a  
415 (INR), IISN project No. 4.4509.10 and Belgian Science Policy under IUAP  
416 VI/11 (ULB). The foundations of Dr. Ezekiel R. and Edna Wattis Dumke,  
417 Willard L. Eccles and the George S. and Dolores Dore Eccles all helped  
418 with generous donations. The State of Utah supported the project through  
419 its Economic Development Board, and the University of Utah through the  
420 Office of the Vice President for Research. The experimental site became  
421 available through the cooperation of the Utah School and Institutional Trust  
422 Lands Administration (SITLA), U.S. Bureau of Land Management and the  
423 U.S. Air Force. We also wish to thank the people and the officials of Millard  
424 County, Utah, for their steadfast and warm support. We gratefully acknowl-  
425 edge the contributions from the technical staffs of our home institutions and  
426 the University of Utah Center for High Performance Computing (CHPC). We  
427 thank HAMAMATSU Photonics K.K., Sanko Seikohjyo Co., Ltd., Quality  
428 Steel Fabricating And Welding, Inc, T&D Maintenance, Nitto Kogyo Cor-

429 poration, and Mitsui Engineering & Shipbuilding Co., Ltd. for their kind  
430 support.

#### 431 **References**

- 432 [1] H. Kawai et al., Nucl. Phys. B Proc. Suppl, 175-176, (2008) 221
- 433 [2] H. Kawai et al., J. Phys. Soc. Jpn. Suppl. A, 78 (2009) 108
- 434 [3] T. Abu-Zayyad et al., NIM A, 450 (2000) 253
- 435 [4] T. Nonaka et al., Proc. of 30th ICRC, 5 (2007) 1005, and now preparing  
436 a detailed paper
- 437 [5] J. N. Matthews et al., Proc. of 30th ICRC, 5 (2007) 1157
- 438 [6] H. Tokuno et al., NIM A, 601 (2009) 364
- 439 [7] H. Tokuno et al., Proc. of 30th ICRC, 5 (2007) 1013, and now preparing  
440 a detailed paper
- 441 [8] Y. Tameda et al., NIM A, 609 (2009) 227
- 442 [9] A. Taketa et al., Proc. of 29th ICRC, 8 (2005) 209, and now preparing  
443 a detailed paper
- 444 [10] P. A. Sadowski et al., Astropart. Phys, 18 (2002) 237

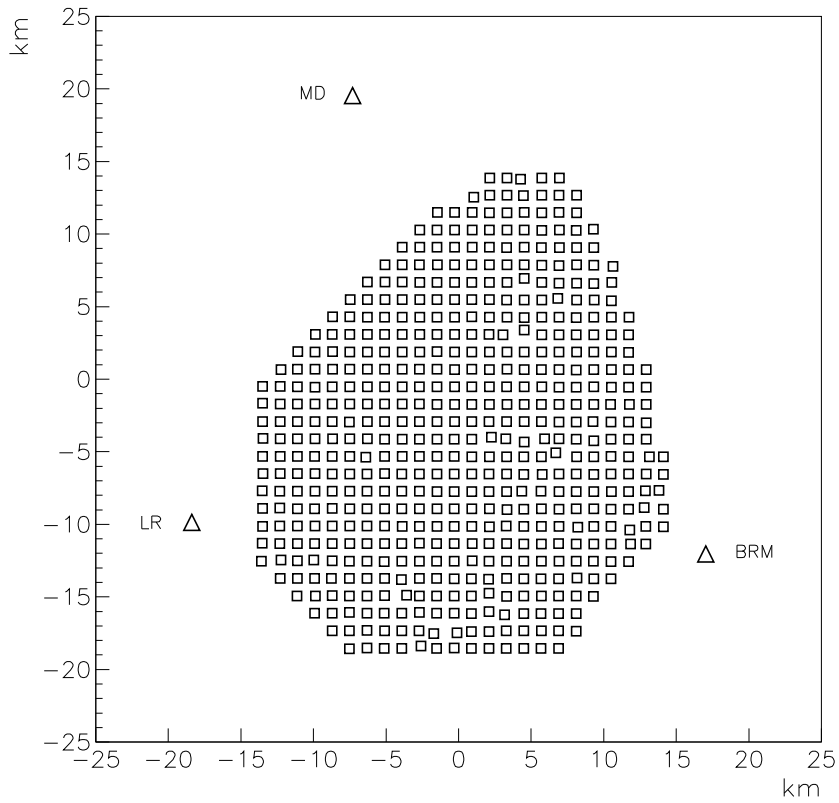


Figure 1: Detector positions in the telescope array experiment. Squares: surface detectors (SDs), triangles: fluorescence detector (FD) telescope stations. SD array area: 700 km, SD spacing: 1.2 km, and distance between FD stations:  $\sim 35$  km.



Figure 2: Picture of the fluorescence detector station.

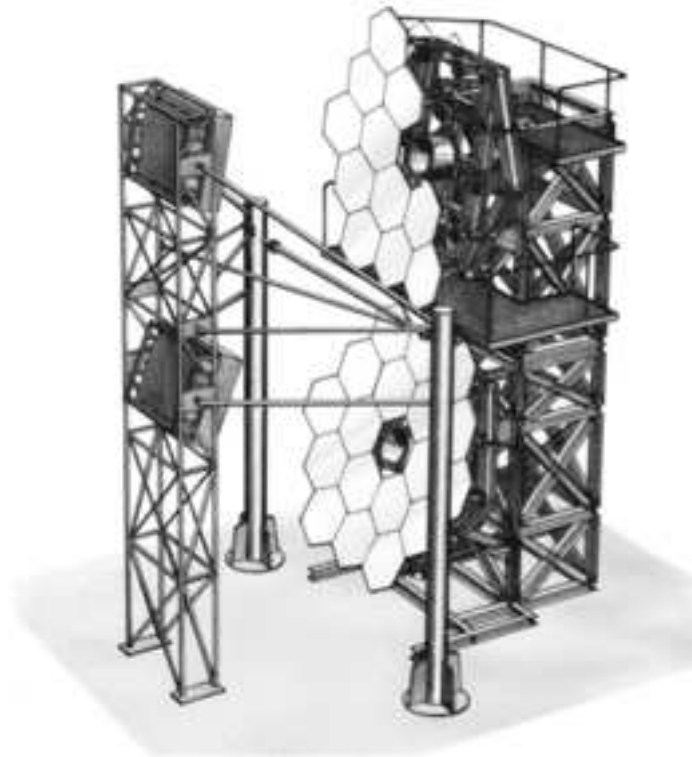


Figure 3: Schematic view of the air fluorescence detectors. For visibility of mirror mounts, seven segment mirrors are removed from the upper telescope.



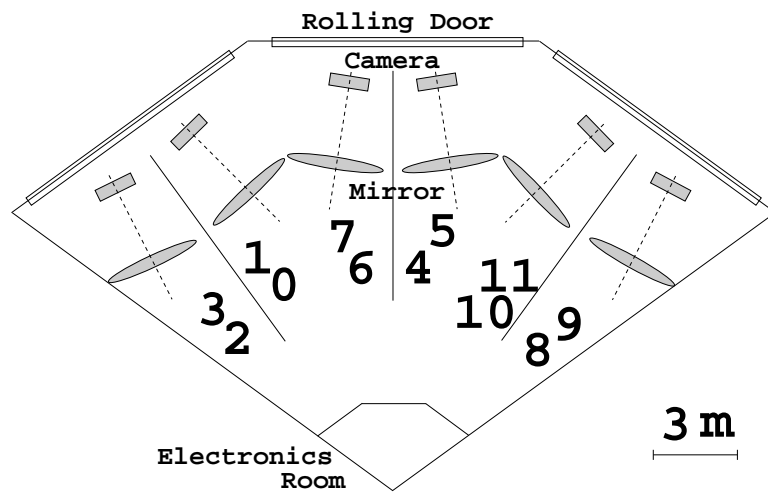


Figure 4: Schematic projected view of the FD station onto the floor (solid lines: datum lines, dashed lines: azimuthal lines of each telescope frame). The telescopes are numbered according to their FOVs, as shown in this figure; the lower (upper) telescopes have even (odd) numbers.

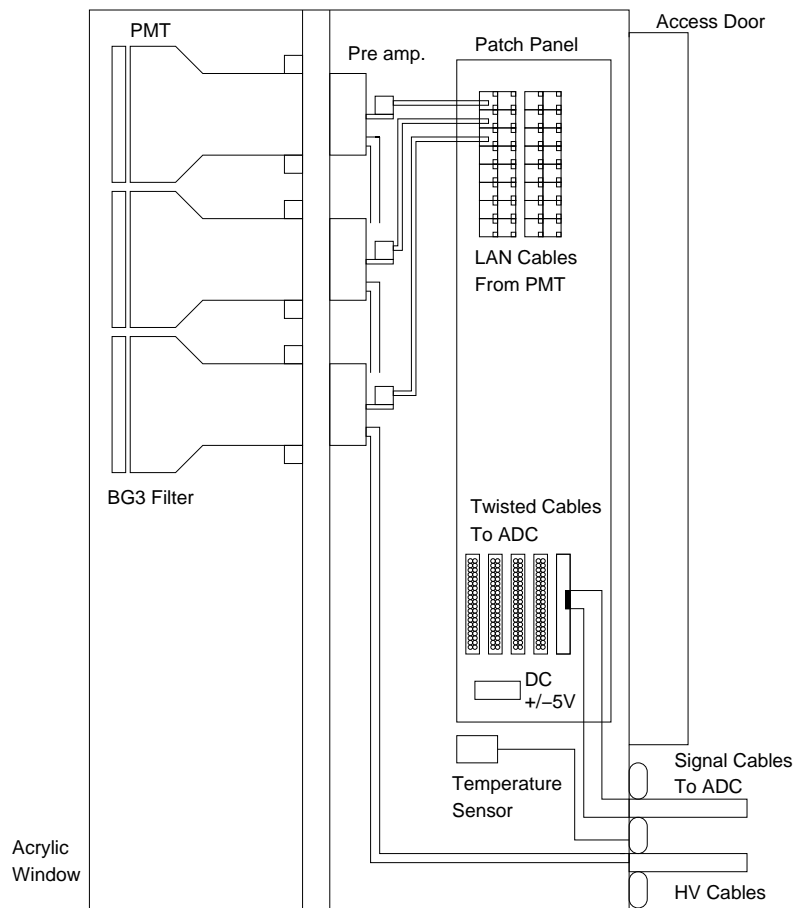


Figure 5: Schematic side view of a PMT camera. Inside the camera, there are 256 PMTs, connected with signal and HV cables, and a temperature sensor.



Figure 6: Rear view of the PMT camera.

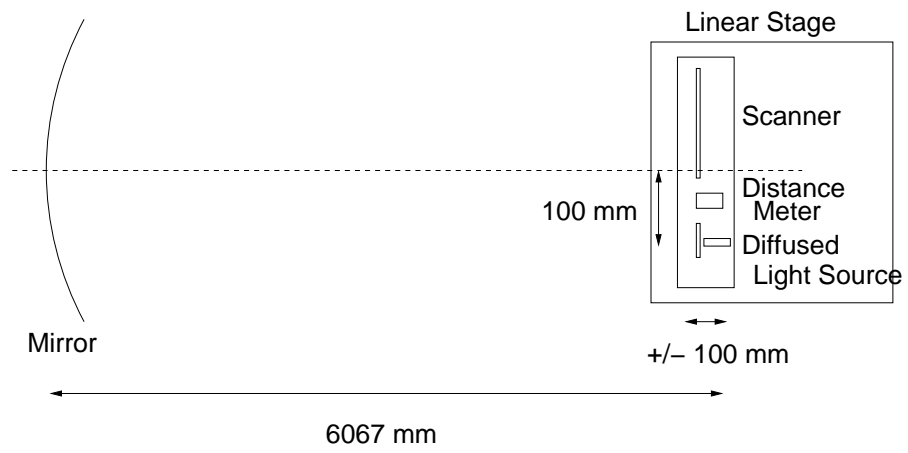


Figure 7: Setup for the measurement of curvature radius of segment mirror.



Figure 8: Photograph of the equipment for measuring the curvature radius of segment mirror. This equipment includes a scanner, a distance meter, and a laser source with a diffuser plate, placed to the right on the linear stage.

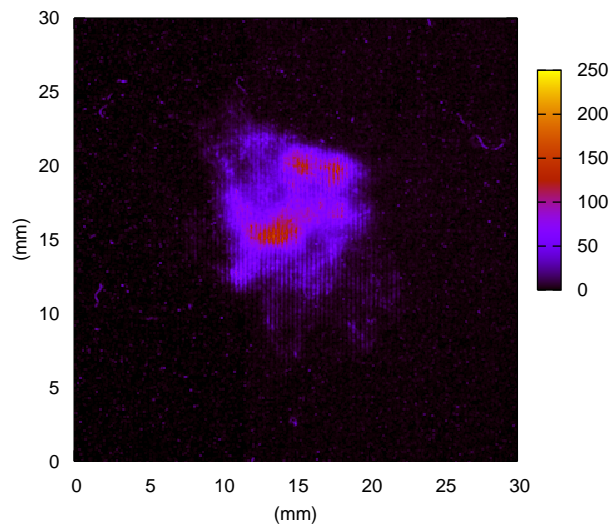


Figure 9: Scanned image of reflected light at the distance equal to the curvature radius of the mirror. Colors show intensities of light in the electrical article.

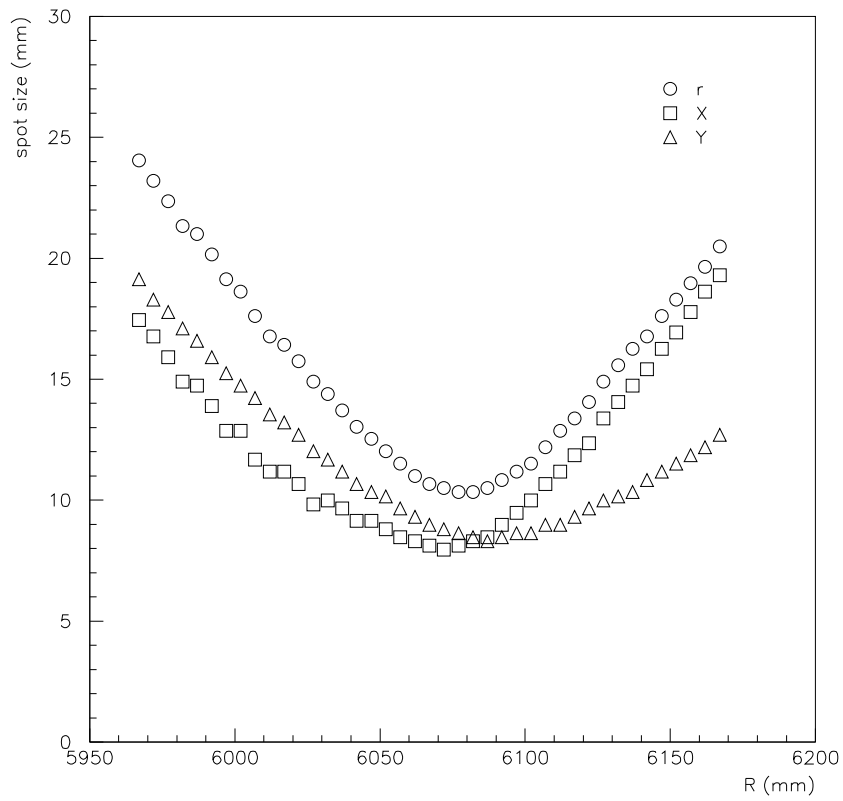


Figure 10: Typical relation between spot size and distance from a segment mirror (circles: spot sizes; squares and triangles: projected spot sizes on X and Y axes, respectively).

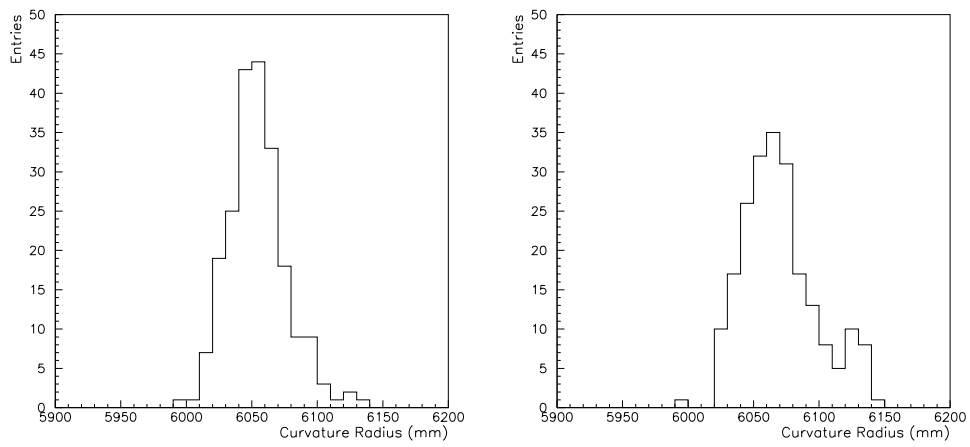


Figure 11: Distribution of the curvature radius of segment mirrors (left: BRM, right: LR).



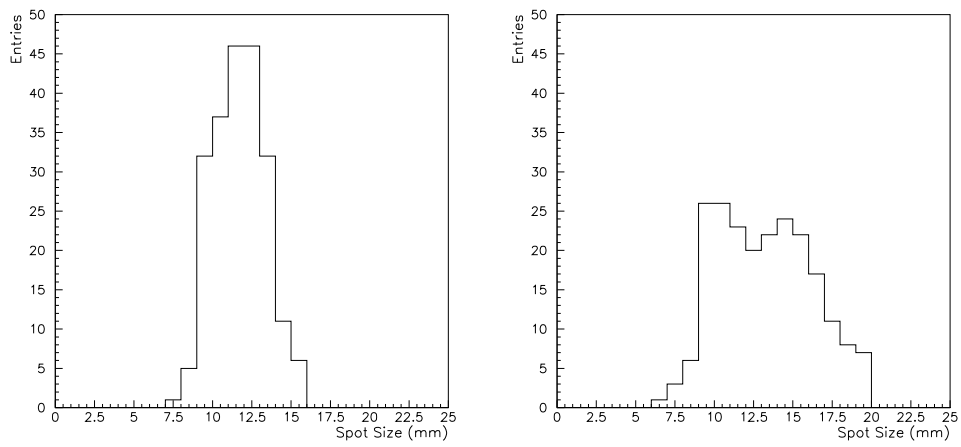


Figure 12: Distribution of the spot size of segment mirrors (left: BRM, right: LR).

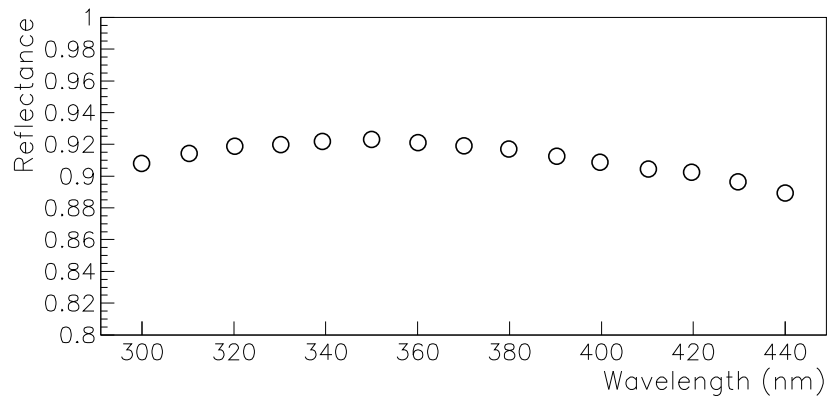


Figure 13: Typical reflectance of small flat mirror, measured by the manufacturer (systematic error and measurement error are less than 1%).

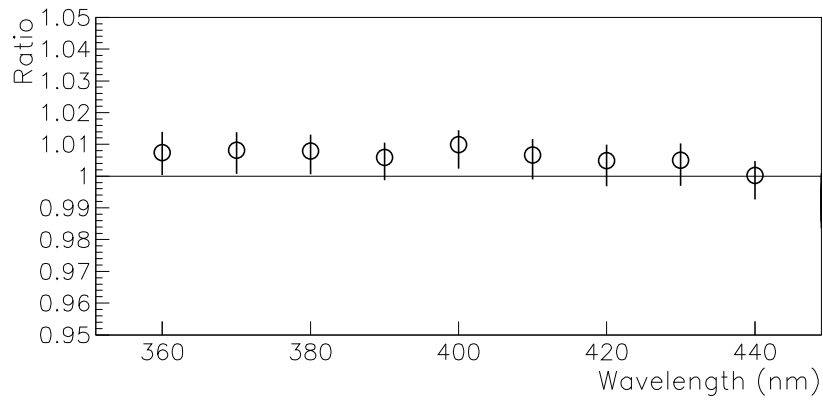


Figure 14: The comparison of mirror reflectance between the NIST measurement and our measurement (plots: our measurement value divided by the NIST one, error bars:  $1\sigma$ ).

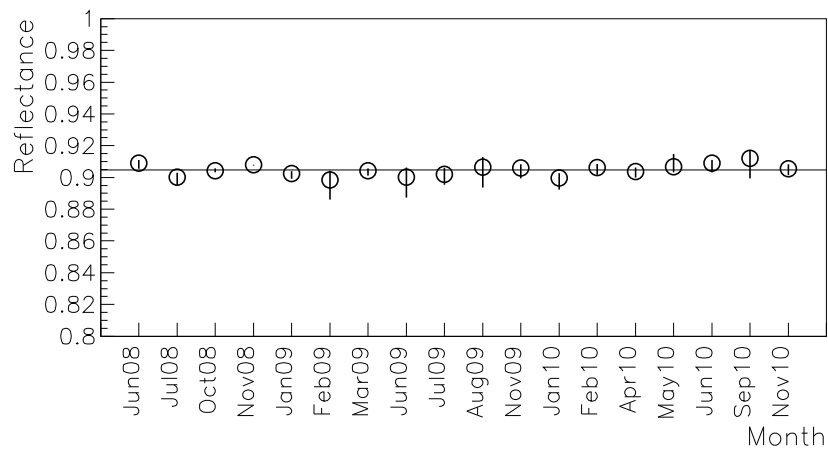


Figure 15: Variation in the reflectance of a reference mirror at 360 nm from June 2008 to November 2010 (plots: median value, error bars:  $1\sigma$ , horizontal line: mean value of the plots).

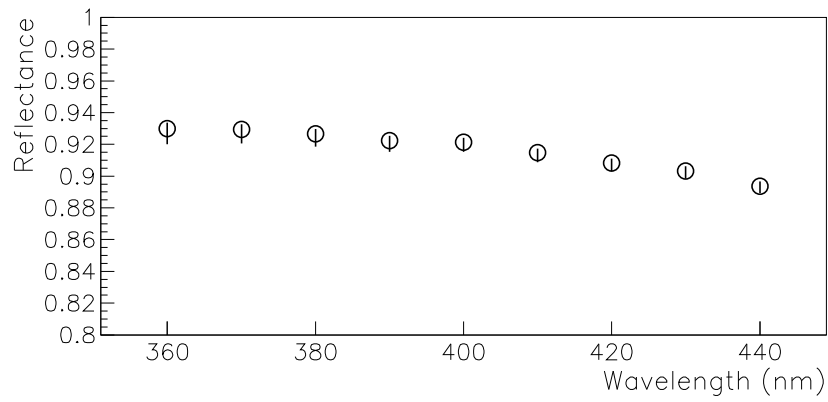


Figure 16: Wavelength dependence of the reflectance of all segment mirrors in March 2007 (plots: median value of 24 primary mirrors, error bars:  $1\sigma$ ).

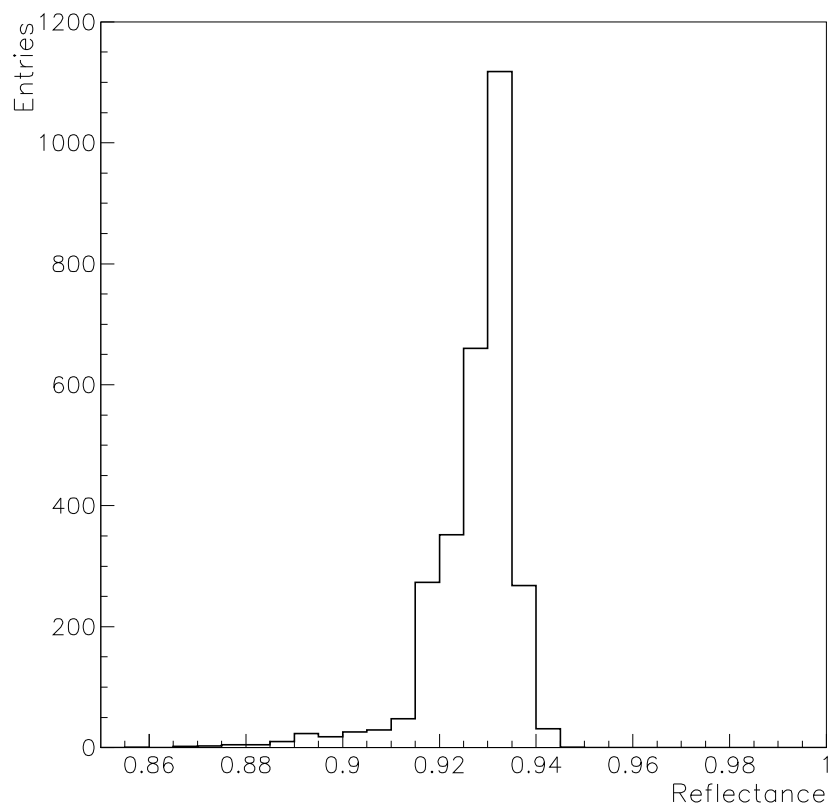


Figure 17: Distribution of mirror reflectance of 24 primary mirrors at 360 nm in March 2007.

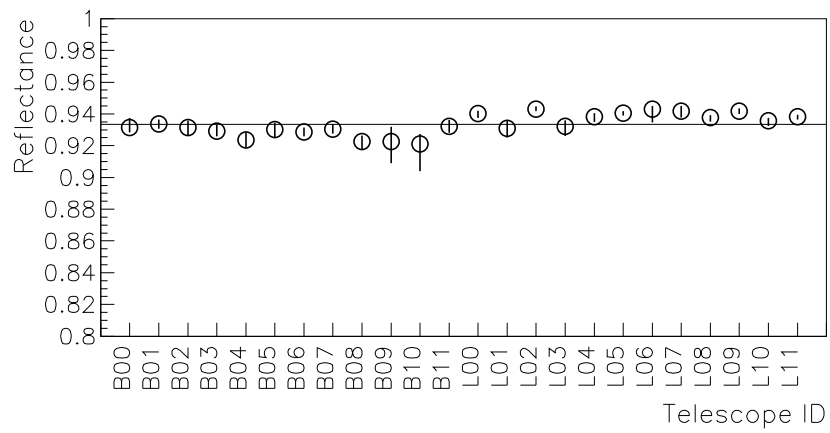


Figure 18: mirror reflectance at 360 nm (horizontal axis: telescope ID, B: BRM, L: LR, plots: median value of 18 segment mirrors, error bars:  $1\sigma$ , horizontal line: mean value of the plots).

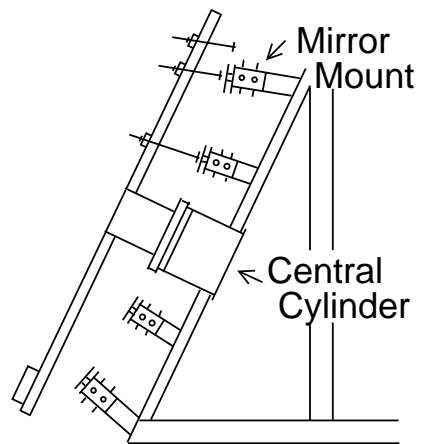


Figure 19: Schematic view of the equipment used for adjusting segment mirror mount. The equipment was mounted on the central cylinder of the mirror.



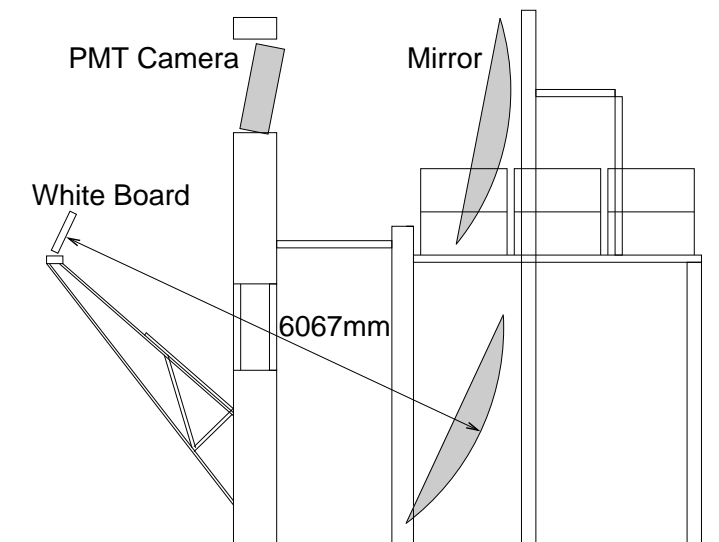


Figure 20: Schematic view of the equipment for adjusting segment mirror direction. The equipment is mounted on a camera support frame. A white board with LEDs is placed at a distance same as the mirror curvature radius of 6067 mm using this equipment.

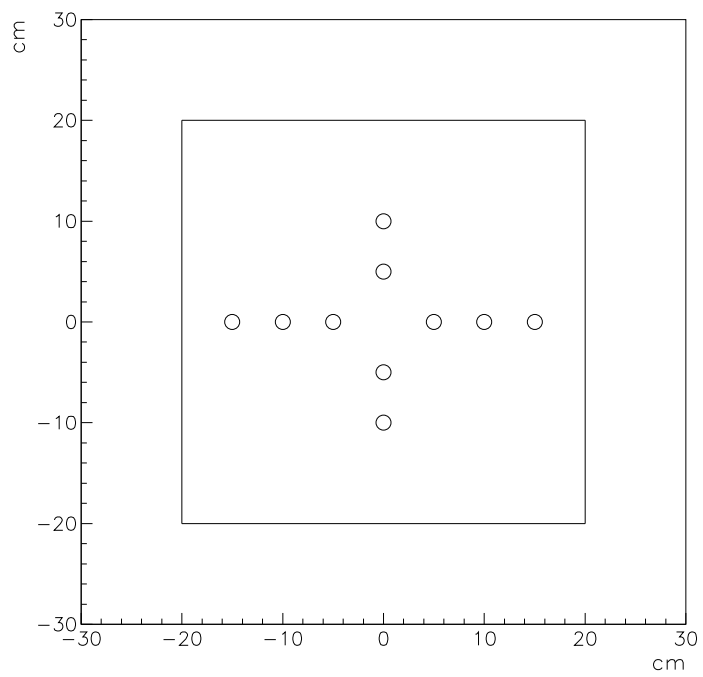


Figure 21: Schematic view of LED positions on the white board of BANANA3.

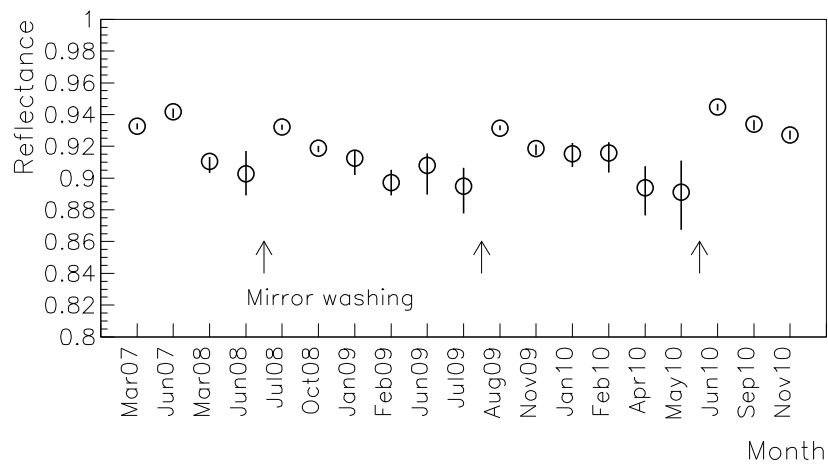


Figure 22: Variation in the mirror reflectance at 360 nm of a typical lower telescope LR04 (plots: median value, error bars:  $1\sigma$ ). The mirror was washed after these measurements in July 2008, August 2009, and May 2010.

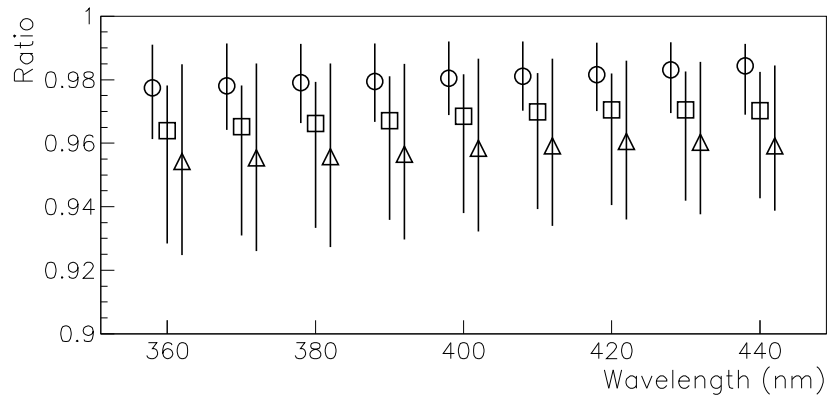


Figure 23: Differences in mirror reflectance before and after mirror washing at each wavelength (ratio: before/after, plots: median value of 24 telescopes, error bars:  $1\sigma$ , circles: 2008, squares: 2009, triangles: 2010). These error bars show the non-uniformity of reflectance just before mirror washing. For visibility, the circles and triangles are slightly moved on the horizontal axis.